

Enhancing Neural Stem Cell Stimulation with Structured Piezoelectric Composites: An In Vitro Study

Vlad Jarkov,* Imaan Waqar, Aleksandar Penev, Chris Bowen, Christopher Adams, and Hamideh Khanbareh*

Spinal cord injuries can cause permanent tissue damage with debilitating and lasting effects on patients. Electrical stimulation has been established as an effective approach for promoting neural regeneration. However, the clinical applicability of these techniques is limited by the necessity for wired connections and external power supplies, which increases risk of infection. Piezoelectric materials have the inherent ability to form electric surface potentials when subjected to a mechanical stress and can provide wireless electrical stimulation. However, current materials are not optimized for neurological applications as they are mechanically mismatched with neural tissue, and have poor biocompatibility. Further, reproducible systems for optimizing material design and stimulation paradigms have yet to be established. Here a new, advanced fabrication process to produce scalable, tuneable piezoelectric ceramic–polymer composites based on $[K_{0.5}Na_{0.5}]NbO_3$ and polydimethylsiloxane is provided. It is demonstrated that these composites can be successfully utilized for the growth of neural stem cells, which are shown to survive, proliferate, retain stemness, and differentiate into their daughter populations. Neuronal differentiation appears to be preferred on poled substrates, in comparison to glass coverslips and unpoled substrates. It is shown that the composites can autonomously generate surface potentials, which opens new possibilities to study piezoelectrically induced electrical stimulation.

1. Introduction

1.1. Neural Stem Cell (NSC) Therapies

Spinal cord injuries (SCI) that result in axonal degeneration and the loss of neurons at the site of injury permanently damage the motor- and sensory-signaling pathways of the body and often lead to life-changing ramifications for patients suffering from these injuries. Currently, there are no cures for spinal injury as rewiring the nervous system in the spinal cord after injury is difficult due to its high degree of complexity.

Stem cell-based transplantation provides a promising avenue for SCI repair as neural stem cells (NSCs) differentiate into the major nervous system cell types, which opens the possibility for potential cell replacement.^[1–3] NSCs can be propagated in culture to generate the required quantity of cells for cell therapy and are associated with high levels of safety; this has resulted in their use in several clinical trials, including for SCI.^[4,5] While NSC transplantation is promising for treatment of SCI, it does face translational challenges such as poor cell survival,^[6] low control over stem cell

differentiation into desired cell types, low levels of integration with existing circuitry, and the need to improve stem cell-mediated release of therapeutic factors.^[7]


1.2. Electrical Stimulation

The application of electrical stimulation has a profound effect on neural transplant cells. For example, it can increase the genesis of nerve cells and guide stem cells to sites of injury,^[8,9] can encourage and direct neural cell growth, and increase the expression of regenerative factors.^[10,11] Generally, electrical stimulation of nervous tissue is provided by external electrodes or electrodes inserted into the spinal cord. However, externally delivered stimulation has a low spatial resolution, potentially leading to off-target effects. Implanted electrodes are often powered by batteries and, once the batteries have reached their end of life, they require surgical replacement, which exposes patients to health risks.

Piezoelectric materials generate electric surface potentials in response to mechanical stimulation, due to their non-centrosymmetric crystal structure. Therefore, they can

V. Jarkov, A. Penev, C. Bowen, H. Khanbareh
Department of Mechanical Engineering
University of Bath
Bath BA2 7AY, UK
E-mail: vj246@bath.ac.uk; hk497@bath.ac.uk

I. Waqar, C. Adams
Department of Neuroscience
School of Life Sciences
Keele University
Staffordshire ST5 5BG, UK

 The ORCID identification number(s) for the author(s) of this article can be found under <https://doi.org/10.1002/adem.202300696>.

© 2023 The Authors. Advanced Engineering Materials published by Wiley-VCH GmbH. This is an open access article under the terms of the Creative Commons Attribution License, which permits use, distribution and reproduction in any medium, provided the original work is properly cited.

DOI: 10.1002/adem.202300696

interact with cells using electrical signals to stimulate tissue repair. Piezoelectric materials have several properties that make them effective for neural stem cell stimulation: 1) Electric field generation: Piezoelectric materials possess the ability to generate an electric field when subjected to mechanical stress. This electric field can be used to stimulate neural stem cells and promote their growth and differentiation; 2) Biocompatibility: Piezoelectric materials are biocompatible, which means they do not harm living tissue and do not trigger an immune response; 3) Non-invasive: Piezoelectric materials can be used in a noninvasive manner, meaning that they can be used to stimulate neural stem cells without requiring invasive procedures or the use of electrodes; 4) High precision: Piezoelectric materials can be engineered with high precision to generate specific mechanical forces and electric fields, which can be tailored to optimize neural stem cell stimulation; and 5) Long-lasting: Piezoelectric materials are also durable and can maintain their properties for extended periods, providing a reliable and long-lasting stimulation platform for neural stem cells.

Conventional piezoelectric ceramics such as lead zirconate titanate (PZT) contain toxic components and are thus not favorable for implantation.^[12] Lead-free ceramics have been shown to be biocompatible with non-neural tissues, such as bone and cartilage.^[13–17] However, the significant mismatch in the mechanical properties of ceramics with those of the nervous system limits their application due to potential additional scarring.^[7,18] Here we propose microstructurally optimized piezoceramic–polymer composites with tuneable properties that can be tailored for modulation of electrically responsive repair processes as a means of functionalizing existing neural implants to improve implant ingrowth and long-term stability. The advantages of piezoelectric ceramic–polymer composites for neural stem cell differentiation and spinal cord regeneration lie in their 1) biocompatibility, ability to provide 2) electrical stimulation, 3) tuneable mechanical properties, 4) enhanced cell adhesion and proliferation, possibility of 5) controlled growth factor release, and their 6) potential to promote neural tissue regeneration.

1.3. Dielectrophoresis (DEP)

Dielectrophoresis (DEP) is the process of exerting a force on a dielectric particle via the application of a nonuniform electric field. Previous research has demonstrated that in particulate composites aligned through dielectrophoresis, enhancing the alignment quality through reduced interparticle distance significantly enhances the piezoelectric properties of the composites.^[19] By improving filler orientation without increasing filler volume fraction, we achieve a high level of electroactive sensitivity while simultaneously preserving the mechanical flexibility of the composites.^[20]

The degree of alignment is subject to the amount dielectrophoretic force (F_{DEP}) applied. F_{DEP} is defined in Equation (1) and is dependent on the permittivity of the polymer matrix (ϵ'_m), the radius of the ceramic particle (r), the radian frequency of the applied field (ω), the applied field (E), and the Clausius–Mossotti factor (k^*), a constant derived from permittivity and conductivity of both the polymer matrix and ceramic particle^[21].

$$F_{DEP} = 2\pi\epsilon'_1 r^3 \text{Re}[k^*(\omega)] \nabla E_{rms}^2 \quad (1)$$

Figure 1 is adapted from studies of Wilson et al.^[22] who observed the structural organization of piezoceramic particles at low-volume fractions in a polymer matrix following DEP. Ceramic particle organization was categorized as follows.

1.3.1. Type I

Large numbers of randomly positioned short chains that are indicative of weak interactions between polarized particles.

1.3.2. Type II

Randomly located “pearl chains” that span the cross-section of the composite are indicative of stronger dielectrophoretic attractive force. Some of these chains show a degree of branching.

1.3.3. Type III

The coalescence of individual chains into aggregated “columns” is indicative of very strong dielectrophoretic attractive force.

Wilson et al. observed that this improvement in alignment is a consequence of the increased field and longer time at constant ceramic loading.

1.4. In Situ Dielectrophoretic Poling (PDEP)

In conventional ferroelectric ceramic–polymer composites, the polymer phase typically exhibits lower permittivity and electrical conductivity compared to the piezoelectric ceramic particles. Consequently, a high AC field at elevated temperatures and extended exposure periods are necessary for effective poling and alignment of ferroelectric domains within the piezoelectric particles (Figure 2a).^[23] Consequently, both the poling process and the resulting effective properties of the composites present

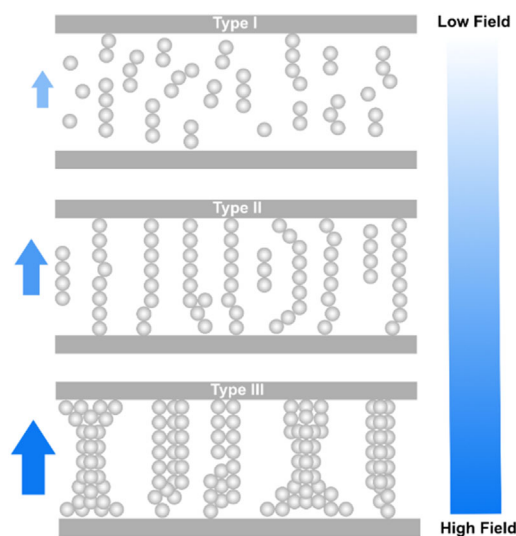


Figure 1. Types of electrically induced structures formed in low-volume fraction piezoceramic composites.^[22] Reproduced with permission [1379839], Copyright 2005, IoP publishing.

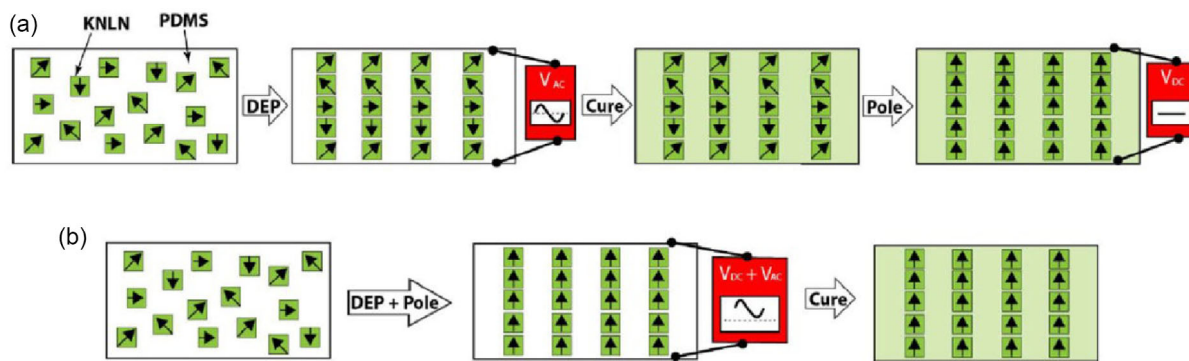


Figure 2. Schematic comparison of a) conventional and b) in situ dielectrophoretic poling (PDEP) procedure for manufacturing of particulate KNN-PDMS composites.

challenges during their production. Recent studies have indicated that the electrical conductivity of the constituent materials significantly influences the dielectric, piezoelectric, and pyroelectric properties of granular composites.^[23] It has been observed that a higher electrical conductivity in the matrix reduces the time required for the electric field to build up on the ceramic particles. Consequently, composites embedded in an electrically conductive matrix can be efficiently poled even at room temperature, with shorter poling durations and relatively lower electric fields. Furthermore, the electrical conductivity and permittivity of the thermoset polymer matrices decrease after curing.

To improve scalability and efficiency of manufacturing, we have developed a new method to perform in situ poling and DEP (PDEP) based on the work of Khanbareh et al,^[24] combining DEP structurization, using an AC electric field, and DC poling while the matrix is in the liquid uncured state can enhance the poling efficiency of the composites (Figure 2b).

In this study, we investigate the manufacture and piezoelectric properties of KNN-based polydimethylsiloxane (KNN-PDMS) composites using a novel technique and assess their compatibility with NSCs and differentiated populations. The composite's piezoelectric response is shown to depend on the grain size, highlighting the possibility to tune the piezoelectric properties by tailoring microstructural features. The in situ poling dielectrophoresis fabrication technique offers a simple and cost-effective approach to manufacture to overcome the difficulties of processing piezoelectric polymers such as PVDF^[25], with potential for scaleup. Cytotoxicity, cell proliferation, and cell viability studies were performed. The cell studies demonstrate low cytotoxicity and enhanced cell viability and proliferation on the composites, compared to a control group. The favorable combination of good piezoelectric performance and low cytotoxicity exhibited by this class of materials emphasizes the potential for active, cell-stimulating implants.

2. Results and Discussion

2.1. X-ray Diffraction

Figure 3 shows the powder diffraction pattern of $[K_{0.5}Na_{0.5}]NbO_3$ (KNN) powder produced via solid-state synthesis. The diffraction pattern was processed on “Qual X”.^[26] Peaks are indexed

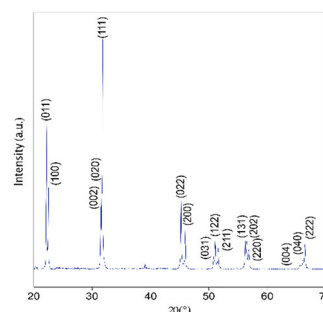


Figure 3. XRD pattern of calcined KNN powder.

according to a phase identifying figure of merit which assesses number of matching peaks, average difference in 2θ peak position, and average difference in peak intensity. The figure shows sharp, well-defined diffraction peaks of a single orthorhombic perovskite phase.

2.2. Particle Size Analysis

Through a double calcination process involving annealing, the KNN particles for 20 h of annealing at 950 °C, while heating at 1 °C min⁻¹, the formation of cuboid particles was observed, as shown in Figure 4. These cuboid particles exhibited small dimensions ranging from 0.5 to 1.0 μm and were characterized by well-defined faceted edges.^[26–28]

2.3. Topological Analysis

Topological analysis was undertaken by tapping mode atomic force microscopy (TM-AFM), which is preferred to contact AFM for softer materials like polymers and composites due to the ultralow force applied to the polymer surface making the technique minimally invasive.^[29] TM-AFM found no difference between the top and bottom surfaces of poled substrates.

2.4. Microstructural Analysis

KNN-PDMS composites produced by PDEP, see Manufacturing of 1-3 using PDEP, at varying ceramic volume fractions

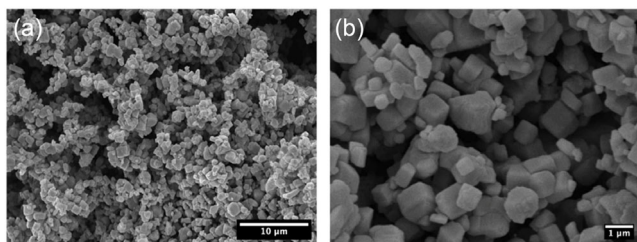


Figure 4. SEM morphological evaluation KNN ceramic powder at a) x2500 and b) x10,000.

(5–15 vol%) and varying AC alignment fields ($1\text{--}2\text{ kV mm}^{-1}$) were examined by SEM. This was undertaken in order to visually characterize differences in ceramic particle alignment and therefore better understand the range of resulting piezoelectric properties when varying these conditions.

2.4.1. Piezoceramic (KNN) Content

Figure 5a–c shows the alignment of ceramic particles at different KNN volume fractions at an alignment field of 2 kV mm^{-1} AC. KNN-PDMS composites containing 5 vol% ceramic (**Figure 5a**) show short chains with poor alignment (**Figure 5a(i)**) and a significant degree of sedimentation (**Figure 5a(ii)**).

As outlined in Equation (3.1), this is likely due to less dielectrophoretic force (F_{DEP}) being applied to the particles due to the lower permittivity of the composite at lower ceramic volume fractions. Composites with 10 and 15 vol% KNN show significantly improved alignment with the formation of clear and distinct particle chains which span the whole cross-section of the sample. Although the degree of alignment is clear in both, there is a significant increase in magnitude of aligned particles between 10 vol% (**Figure 5b**) and 15 vol% (**Figure 5c**).

2.4.2. AC Alignment Field

Figure 6a,b shows the alignment of ceramic particles at different AC alignment fields ($1\text{--}2\text{ kV mm}^{-1}$). **Figure 3** and **6a** shows

alignment under 1 kV mm^{-1} resembles Type I alignment, having a mixture of dispersed particles (**Figure 6a(i)**) and randomly positioned smaller chains (**Figure 6a(ii)**). Furthermore, there is a large degree of topological imperfections within distributed chain continuity (**Figure 6a(iii)**) which can have a detrimental effect of piezoelectric properties.^[30] Composites aligned under 2 kV mm^{-1} (**Figure 6b**) resembled Type II structures with longer, highly ordered ceramic chains (**Figure 6b(i)**), even verging on Type III structures with areas of clear chain coalescence (**Figure 6b(ii)**).

2.5. Dielectric and Piezoelectric Properties: In Situ Dielectrophoretic Poling (PDEP) Studies

These studies are built upon the work of Deutz et al^[31] composites, in which they observed a tenfold increase in dielectric properties between randomly dispersed (0–3) and dielectrophoretically aligned (pseudo 1–3) KNN-PDMS composites, following poling at 7.5 kV mm^{-1} ($150\text{ }^{\circ}\text{C}$, 6 mins). Composites manufactured by PDEP were produced in batches of 16 samples and characterized by relative permittivity (ϵ_r), and the piezoelectric charge coefficients (d_{33}), and voltage coefficients (g_{33}).

Figure 7a–c shows the effect of varying KNN content (5–15 vol%) at different DC poling fields ($2\text{--}3\text{ kV mm}^{-1}$), and **Figure 7d–f** shows the effect of varying DC poling field ($2\text{--}3.5\text{ kV mm}^{-1}$) at different AC alignment fields ($1\text{--}2\text{ kV mm}^{-1}$) for 10 vol% KNN-PDMS composites. During the study, we observed that a combined AC and DC field that was greater of equal to 5 kV mm^{-1} resulted in breakdown and short circuiting of the electrodes. This manifests as a sudden and rapid increase in voltage, which was seen in the attenuation signal from both the amplifier and across the sample, see **Figure S1**, Supporting Information. This breakdown resulted in either the partial or complete decomposition of the composites and left composites burned or uncured, see **Figure S2**, Supporting Information. Finally, we observed a significant amount of sedimentation when applying an AC alignment field of greater or equal to 1 kV mm^{-1} for longer than 2 h which results in a decrease in piezoelectric properties (d_{33} and g_{33}), see **Figure S3**, Supporting Information.

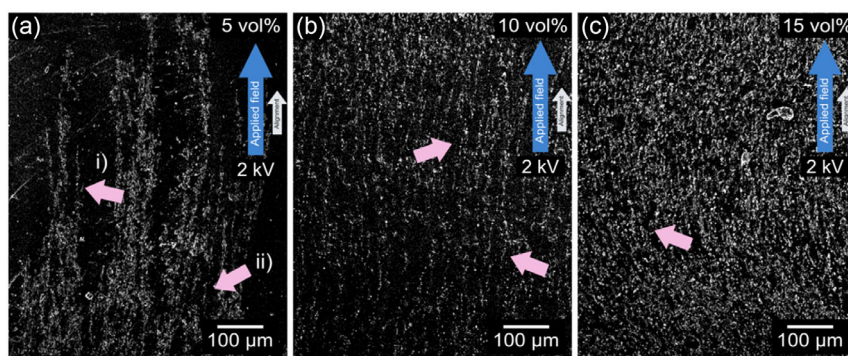


Figure 5. SEM images showing particle alignment in a) 5 vol%, b) 10 vol%, and c) 15 vol% KNN-PDMS composites aligned via PDEP at 2 kV mm^{-1} . Pink arrows indicate regions of interest referred to in the text; (i) shows regions of broken chain alignment and (ii) shows significant sedimentation in KNN-PDMS composites.

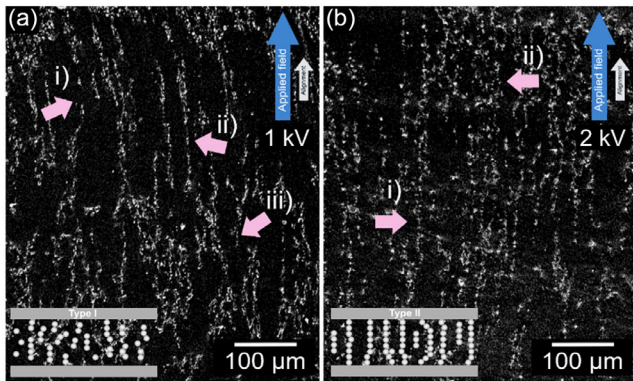


Figure 6. SEM images showing particle alignment of 10 vol% KNN-PDMS composites via PDEP at a) 1 kV mm^{-1} with regions of (i) dispersed particles and (ii) smaller randomly positioned chains indicative of Type I alignment and b) 2 kV mm^{-1} AC alignment fields with (i) highly ordered ceramic chains indicative of Type II alignment and (ii) areas of clear chain coalescence indicative of Type III alignment.

2.5.1. Piezoceramic (KNN) Content

Figure 7a–c shows the effects of KNN content (5%–15%) on the dielectric (ϵ_r) and piezoelectric properties (both d_{33} and g_{33}) of the composites after PDEP-poling at 2 kV mm^{-1} AC and 2 kV mm^{-1} DC. The relative permittivity increases almost linearly with increasing ceramic volume fraction and is independent

of poling field. Piezoelectric properties, which otherwise follow the same trend, exhibit a peak at 10 vol% KNN (3 kV mm^{-1} DC, 2 kV mm^{-1} AC) with a $d_{33} = 11 \pm 1.5 \text{ pC N}^{-1}$ and $g_{33} = 202 \pm 25.5 \text{ mV N}^{-1}$, respectively. This is due to the superior particle alignment observed in 10 vol% KNN compared to 5 and 15 vol% and is characterized by more continuous percolating chains, see Microstructural Analysis section. This aligns with the observations of both Deutz et al.^[31] and Khanbareh et al.^[24] in their studies of similar DEP aligned KNN-PDMS and PDEP PZT-PDMS composites. The 10 vol% KNN-PDMS composites were therefore selected to undergo further study due to their superior piezoelectric properties.

2.5.2. Poling (DC) and Alignment Field (AC)

Figure 7d–f shows the effects of both DC poling field and AC alignment field on the dielectric and piezoelectric properties of 10 vol% KNN-PDMS composites. The relative permittivity remained constantly independent of both poling and alignment fields due to the unchanging KNN volume fraction. Higher AC alignment field resulted in significant increases in piezoelectric properties at the same and higher DC poling fields. The 10 vol% KNN composites at an AC alignment field 2 kV mm^{-1} ($d_{33} = 12 \pm 1.3 \text{ pC N}^{-1}$ and $g_{33} = 195 \pm 34.0 \text{ Vm N}^{-1}$) exhibited improved piezoelectric properties compared to composites aligned at 1 kV mm^{-1} when poled at 3 kV mm^{-1} ($d_{33} = 7 \pm 1.0 \text{ pC N}^{-1}$ and $g_{33} = 128 \pm 14.9 \text{ Vm N}^{-1}$) and 3.5 kV mm^{-1} respectively ($d_{33} = 8 \pm 0.64 \text{ pC N}^{-1}$ and $g_{33} = 155 \pm 41.0 \text{ Vm N}^{-1}$),

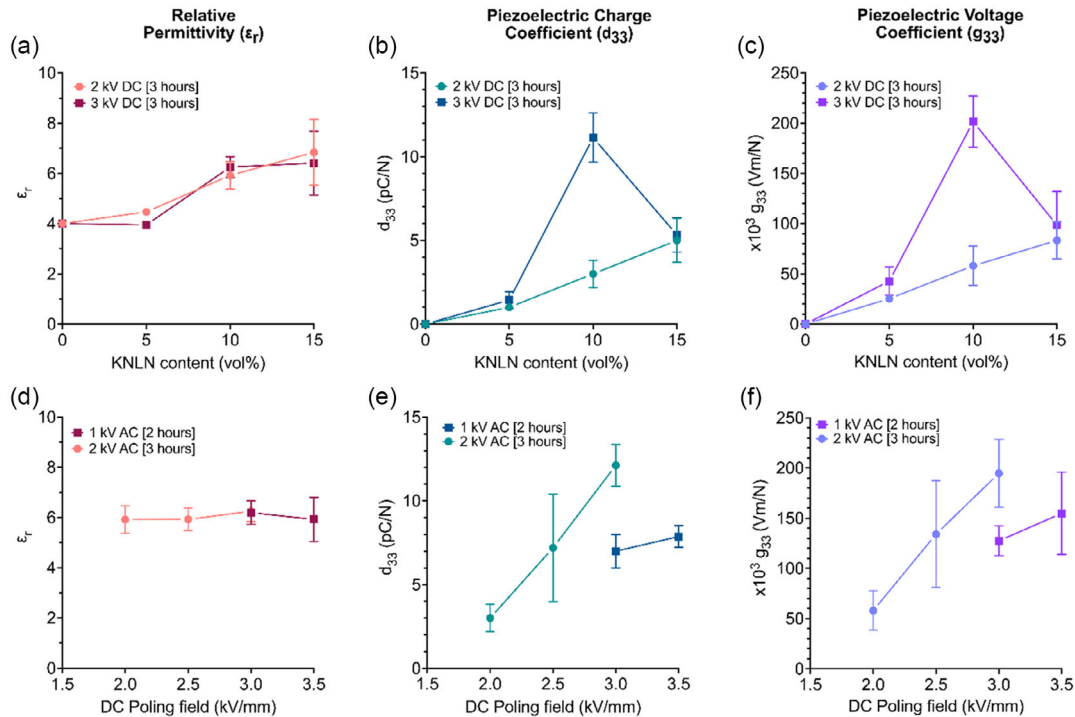


Figure 7. Studies in dielectric and piezoelectric properties of 1–3 KNN piezoelectric composites produced by in situ dielectrophoretic poling. The first row shows a) permittivity (ϵ_r), piezoelectric b) charge (d_{33}), and c) voltage (g_{33}) coefficients as a product of varying ceramic volume fraction (5–15 vol%) after poling at 2 kV mm^{-1} (pink) and 3 kV mm^{-1} (maroon) DC for 3 h at 2 kV mm^{-1} AC. The second row shows the d) permittivity (ϵ_r), piezoelectric e) charge (d_{33}), and f) voltage (g_{33}) coefficients of 10 vol% KNN-PDMS composites at varied DC poling fields 2 to 3.5 kV mm^{-1} and AC alignment fields, 1 and 2 kV mm^{-1} .

respectively. This study demonstrates the successful batch manufacturing of KNN-PDMS composites with varied piezoelectric properties. The methods make it possible to consistently reproduce samples with varied piezoelectric properties to test the effects of piezoelectric stimulation of neural stem cells

2.6. Mechanical Properties of the Substrates

The mechanical properties were evaluated using DMA. A Triton 2000 DMA machine equipped with a tension mode clamp fixture is used in tension at 1 Hz to characterize the viscoelastic behavior of the samples. The storage modulus was measured to be 1 MPa at 25C.

The mechanical properties of a piezoelectric substrate can affect the behavior and differentiation of cells grown or implanted on it. The mechanical properties of the substrate, such as stiffness or elasticity, can affect the forces that the cells experience, which can, in turn, affect cell adhesion, migration, and differentiation. For neural stem cells, the mechanical properties of the substrate could potentially affect the differentiation of the stem cells into specific neural cell types or influence dendritic and axonal outgrowth. It is critical to maintain their viability and promote their differentiation into mature neural cells. A study by Li et al. demonstrated that neural stem cells cultured on soft substrates exhibited higher proliferation rates than those on stiff substrates (Li et al, *Biomaterials*. 34(31):7616-25, 2013). Another study showed that neural stem cells cultured on substrates with high elasticity exhibited more differentiation into neurons compared to those on less elastic substrates (Blaschke et al, *Tissue Eng Regen Med.*;13(6):960-972. 2019). However, more research is needed to understand the extent and specificity of these effects on the stimulation of neural stem cells implanted on piezoelectric substrates.

2.7. Neural Stem Cell (NSC) Studies

In the following studies, we derive NSCs from the subventricular zone of P₀ mice and propagate as neurospheres, under growth

factor drive (EGF and FGF-2). The neurospheres were then dissociated and cultured on poled and unpoled 10 vol% KNN-PDMS ($d_{33} \geq 8 \text{ pC N}^{-1}$). To examine the effect of materials on the NSC population, NSCs were cultured on the materials in NSC medium for up to four days. Subsequently, the medium was switched to differentiation medium (no growth factors/1% fetal bovine serum) for seven days to examine how the scaffolds affect NSC differentiation. Both poled and unpoled composites were tested (alongside standard glass coverslips) to determine differences in stem cell behavior on piezoelectrically active and inactive substrates. Sample were purposefully left uncoated to ensure the effect of electrical stimulation was not masked by the addition of surface proteins like laminin.

2.7.1. NSC Cytocompatibility

NSC health was evaluated threefold, as a product of proliferation (EdU) and stemness (nestin, sox-2), and the results are summarized in **Figure 8**.

After culture in NSC medium, the majority of cells were clearly positive for nestin and Sox-2. The staining profiles were similar to those observed in previous studies, with nestin marking the cytoskeleton and the transcription factor Sox-2 restricted to the nucleus. Cells appeared to grow across all conditions, although there was significant heterogeneity in cell distribution. This was most pronounced on the unpoled substrates where NSCs appeared to grow as neurospheres. Figure 8a–d shows nestin staining across all conditions. We estimated nestin to be present in over 90% of the population, but absolute quantification was not possible as individual cells could not be differentiated across the repeated conditions. In one experiment, we also confirmed NSC proliferation through EdU staining which was present in all conditions, Figure 8a–d. Figure 8e–h shows Sox-2 was present in all conditions with > 80% of cell positive, coverslip $81.3\% \pm 7.93\%$, unpoled $88.9\% \pm 10.78\%$, positively poled $92.6\% \pm 6.59\%$, and negatively poled $95.3\% \pm 3.53\%$ with no significant difference between substrates ($p > 0.05$, $n = 3$).

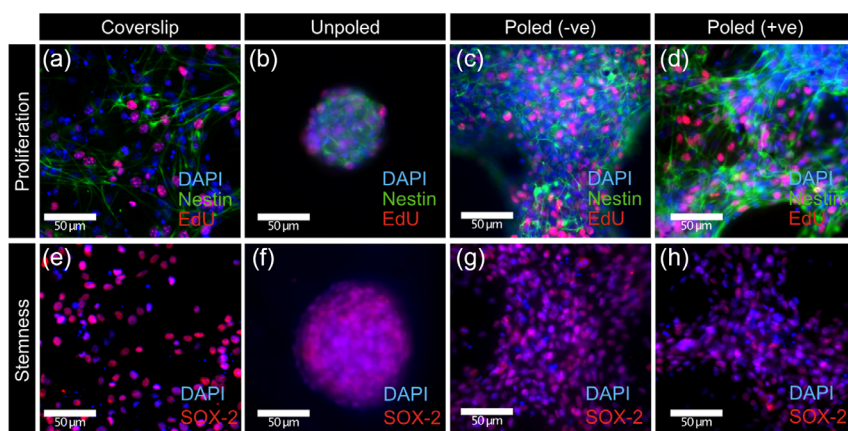


Figure 8. NSCs were successfully cultured on all substrates and showed a high degree of both stemness (>80%) and cytocompatibility (<85%) with no significant difference between conditions ($p > 0.05$, $n = 3$). Nestin and EdU stained NSCs on a) glass and b) unpoled, c) negatively poled (–ve) and d) positively poled (–ve) 10 vol% KNN-PDMS. Sox-2 stained NSCs on e) glass and f) unpoled, g) negatively poled (–ve) and h) positively poled (–ve) 10 vol% KNN-PDMS.

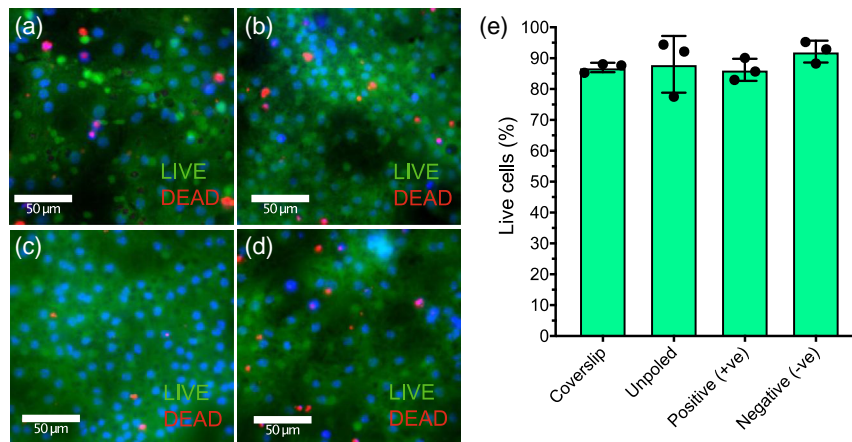


Figure 9. NSCs were successfully differentiated on all substrates and showed a high level of viability. Live/dead assay of differentiated NSCs on a) glass and b) unpoled, c) negatively poled (–ve) and d) positively poled (–ve) 10 vol% KNN-PDMS. Bar graph e) summarized the viability of the cells on different substrates.

It should be noted that NSCs on unpoled KNN-PDMS were less homogeneously distributed and tended to remain in neurospheres on the surface of the composites and is clearly displayed in Figure 8b,f. This indicates that poled composites are better at facilitating the migration of NSCs in a similar manner to extracellular matrix molecules such as laminin,^[32,33] although this is not necessarily an advantage in neural tissue engineering as neurospheres have shown higher survival rates following transplantation.^[34] **Figure 9** shows that the NSCs were successfully differentiated on all substrates and showed a high level of viability.

2.7.2. Differentiated NSCs Health

Differentiated NSC health was evaluated as a product of cell viability (live/dead) assays, and the results are summarized in Figure 9.

Figure 9a–e shows NSCs in all conditions had high viability (>85%) with no significant difference between conditions ($p > 0.05$, $n = 3$). The majority of cells had taken up the live (green) stain with a few dead (red) cells, distributed throughout.

2.7.3. Differentiated NSCs Studies

Immunocytochemistry revealed that the NSCs had successfully differentiated in all conditions into the expected phenotypes: neurons (**Figure 10a–d**), oligodendrocytes (**Figure 10e–h**), and astrocytes (**Figure 10i–l**).

Figure 10m shows that there is an increase in neurogenesis on the poled scaffolds, and this is significant for the positive (+ve) condition ($p < 0.005$, $n = 3$) versus the unpoled condition. This trend indicates that the remnant polarization and/or the mechanical deformation of the scaffolds during cell culture is sufficient to facilitate an increase in the differentiation of NSCs into neurons. There was no significant difference between proportions or astrocytes (**Figure 10n**) and oligodendrocytes (**Figure 10o**) on all substrates ($p > 0.05$, $n = 3$).

The effect of poling on neural stem cells is believed to be due to the response of the cells to the electric field. The electric field

can influence the expression of genes involved in neural differentiation and maturation. The mechanisms underlying these effects include the piezoelectric field enhancing the cell membrane's permeability, influencing cell signaling and gene expression, and modulating the cytoskeleton dynamics. This influence is not present in the unpoled substrates as there is no electric field present. However, all other chemical, mechanical, and topological properties of the unpoled substrates are similar to the poled substrates.

Overall, poling a piezoelectric material can provide a useful tool for manipulating the behavior of neural stem cells, which has potential applications in regenerative medicine and tissue engineering. While the mechanisms behind the influence of poling on the differentiation of neural stem cells in piezoelectric materials are still not fully understood, it is believed that the electric fields generated by the poling process can alter the behavior of the cells, regulating their differentiation into specific neuronal lineages. One proposed mechanism is that the electric fields generated by the poling process can induce changes in the cell membrane potential, which can then activate intracellular signaling pathways that regulate gene expression and cell fate determination. This can lead to the differentiation of neural stem cells into specific neuronal subtypes, such as motor neurons or sensory neurons. Another proposed mechanism is that the electric fields generated by the poling process can directly stimulate the differentiation of neural stem cells by promoting the formation of neurites and axons. This can lead to the development of more mature and functional neuronal networks, which are essential for proper neural function.

While the exact mechanisms behind the influence of poling on the differentiation of neural stem cells in piezoelectric materials are still being examined, it is clear that the electric field generated by the poling process can have a significant impact on the behaviour of these cells and provides a novel approach for the development of tissue engineering and regenerative medicine therapies for neurological diseases and injuries.

The potential mechanisms behind the enhancement of neural stem cell stimulation by piezoelectric composites can include

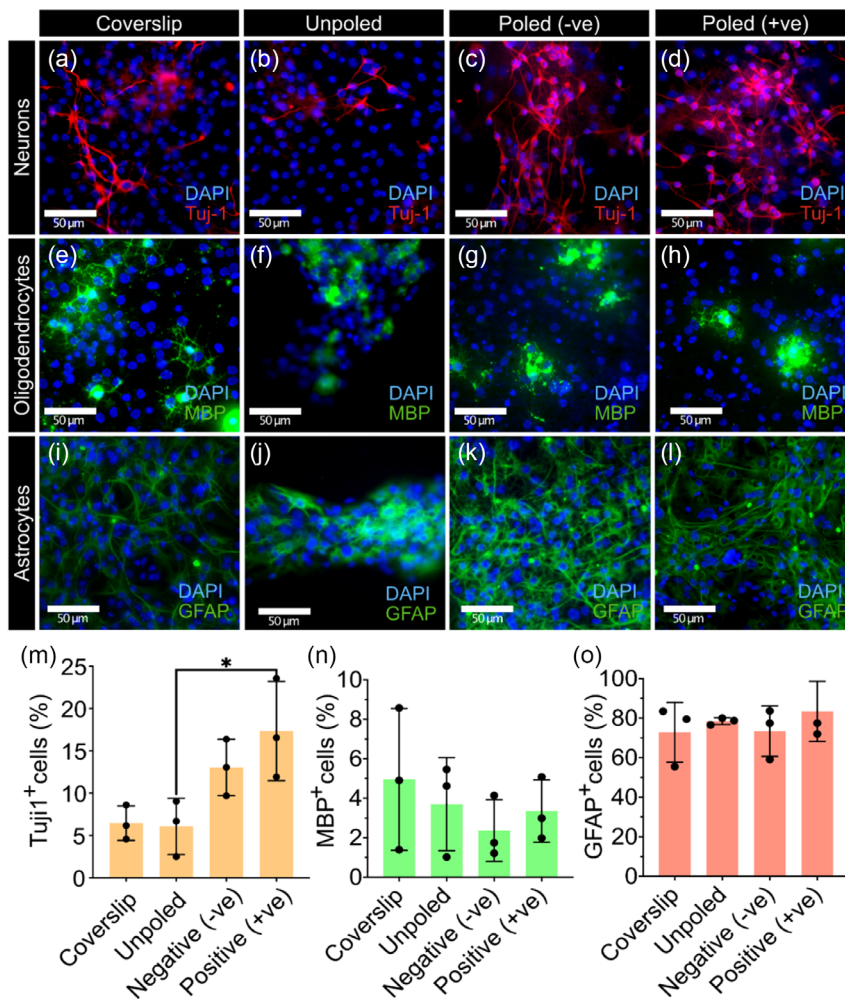


Figure 10. NSCs were successfully differentiated into phenotypical cell types on all substrates and showed a significant increase in neurogenesis in the positively (+ve) poled condition. Tuji-1 stained NSCs on a) glass and b) unpoled, c) negatively poled (-ve) and d) positively poled (-ve) 10 vol% KNN-PDMS. MBP stained NSCs on e) glass and f) unpoled, g) negatively poled (-ve) and h) positively poled (-ve) 10 vol% KNN-PDMS. GFAP MBP stained NSCs on i) glass and j) unpoled, k) negatively poled (-ve) and l) positively poled (-ve) 10 vol% KNN-PDMS. Bar graph m-o) showing the proportion of each cell phenotype where * indicates values significantly different to the unpoled condition ($p < 0.005$, $n = 3$).

piezoelectric effects, biophysical cues, and synergistic effects with other stimuli, meaning that piezoelectric composites may amplify the effects of other stimuli, such as electrical fields, magnetic fields, or biochemical signals. This could lead to more efficient and effective neural stem cell stimulation and potentially open up new avenues for cell-based therapies or tissue engineering approaches.

Overall, the mechanism behind the enhancement of neural stem cell stimulation by piezoelectric composites is likely multifactorial and complex and could involve a range of biochemical, biophysical, and mechanical processes. Further research is needed to fully elucidate this mechanism and optimize the use of piezoelectric composites for neural stem cell applications.

In addition, the piezoelectric composites can be tailored to provide specific electrical properties that match the neural stem cells' electrical environment, facilitating their growth and differentiation. The combination of the piezoelectric field's physical

and electrical stimulations is believed to promote the neural stem cells' development into specific neuronal phenotypes. Moreover, the use of piezoelectric composites eliminates the need for exogenous chemical factors, such as growth factors, that might compromise the cell's fate or affect other processes, reducing the adverse effects associated with the traditional methods. The reproducibility, scalability, and cost-effectiveness of piezoelectric composites make them ideal for neural tissue engineering applications.

3. Conclusions and Future Perspectives

This work shows the first demonstration of a successful batch production of $[K_{0.5}Na_{0.5}]NbO_3$ -based polydimethylsiloxane (KNN-PDMS) composites with large and highly tailorable piezoelectric properties, $d_{33} = 3\text{--}12 \text{ pC N}^{-1}$ and $g_{33} = 58\text{--}195 \text{ Vm N}^{-1}$, produced via a novel in situ dielectrophoretic poling technique.

These tailorable properties are achieved by simply changing the DC poling field during in situ poling-dielectrophoresis (PDEP).

While the literature to date has shown that piezoelectric stimulation can increase neuronal differentiation (SHY-SYSY),^[35] neurogenesis (PC12),^[36] and enhance neurite outgrowth (mixed spinal culture and dorsal root ganglion neurons)^[37,38] and sprouting (PC12),^[39] they focus on the materials employed rather than the details of the stimulation itself. Further, reproducible systems for optimizing material design and stimulation paradigms have yet to be established. The work outlined here provides an electrically facile system that can be produced at batch scale and can be used to explore the gaps and minutia of PIES and how it varies with varied electrical input.

The KNN-PDMS composites not only show high cytocompatibility (>80%) but they also support the differentiation of NSCs, and the +ve poled composites are shown to facilitate neurogenesis. These new materials are therefore a promising conduit to explore the impact of piezoelectrically induced electrical stimulation on, therapeutically relevantly, stem cells which tend to suffer from poor cell survival,^[6] low control over stem cell differentiation into desired cell types.^[7] These composites can therefore be used as a tool to understand both the degree and extent PIES can play in neural regeneration more widely. The novel piezoelectric composites have potential to be incorporated into a flexible implantable device that can be placed over the spinal cord. When the device is stretched or compressed due to spinal cord movement, it generates an electrical signal that can stimulate the cells in the spinal cord and promote regeneration. The electrical stimulation provided by the piezoelectric composites can also help to activate specific pathways in the spinal cord that are involved in regeneration. This can facilitate the growth and differentiation of stem cells, which are important for the regeneration of damaged spinal cord tissue.

In summary, we provide the first demonstration that piezoelectric particulate composites can be successfully utilized for growth of primary neural stem cells (NSCs), which are shown to survive, proliferate, retain stemness, and differentiate into their daughter populations on the composites. Neuronal differentiation appears to be preferred on poled substrates, in comparison to glass coverslips and unpoled substrates. We show that the composites can autonomously generate electric surface potentials, which opens new possibilities to study piezoelectrically induced electrical stimulation. The use of piezoelectric materials, such as these, in regenerative medicine can lead to the development of new therapies and treatments for neurodegenerative disorders and nerve injuries. By promoting the differentiation and migration of neural stem cells, the materials can potentially help to replace damaged or lost neurons in the brain, thereby restoring lost neural function. Overall, the use of piezoelectric materials in neural stem cell research holds great promise for advancing our understanding of neural development and repair and developing new therapies for neurological diseases.

4. Experimental Section

Piezoceramic Powder Synthesis: To synthesize a ferroelectric and piezoelectric ceramic potassium sodium niobate (KNN) powder, a solid-state reaction method was employed using a composition of $[\text{K}_{0.5}\text{Na}_{0.5}]\text{NbO}_3$ and $\text{K}_{0.485}\text{Na}_{0.485}\text{Li}_{0.03}\text{NbO}_3$. Stoichiometric amounts of the 99% pure

oxides NaCO_3 , K_2CO_3 , Nb_2O_5 , and/ or Li_2CO_3 (obtained from Sigma Aldrich) were immersed in ethanol and subjected to milling in glass jars using 5 mm yttria-stabilized ZrO_2 balls. A two-step calcination scheme was employed to obtain cuboid particles.^[40] Initially, the KNN powder was calcined at 1050 °C for 3 h, with a heating rate of 5 °C per minute, followed by a milling duration of 5 h. Subsequently, the powder was subjected to a second calcination at 950 °C for 20 h, with a heating rate of 1 °C per minute. Ultrasonication for 1 h was performed to disperse loose aggregates, and the calcined powders were sifted through a 63 μm mesh. The resulting KNN powder was then dried overnight at 150 °C and stored under vacuum at room temperature until further processing into composites.

Manufacturing of 1–3 Using In Situ Dielectrophoretic Poling (PDEP): KNN-PDMS composite films were fabricated by blending KNN microcubes with a two-component PDMS polymer (Sylgard 184, Dow Corning) in a volume ratio of 10%. The mixture was degassed and poured into a prepared Teflon mould, which was then clamped between two steel plates. In order to achieve alignment of the KNN microcubes within the uncured PDMS, an in situ poling dielectrophoresis method was employed, as illustrated in Figure 2b. An AC electric field of 2 kV mm⁻¹ was applied during the alignment process. The effectiveness of dielectrophoresis alignment was determined by analyzing the phase angle between the applied voltage and leakage current at various frequencies ranging from 1 mHz to 10 kHz. The optimal frequency, where the phase angle reached 90°, indicated the highest degree of alignment and minimal leakage current, thus achieving a predominantly capacitive behavior in the composite slurry. However, due to factors such as the electrical properties of the matrix and filler, matrix viscosity, and filler morphology, incomplete alignment was observed with typical phase angles ranging from 50° to 60°. At a frequency of 200 Hz, an optimal phase angle of 88° was achieved, indicating a high degree of alignment. After one hour, the films were cooled to room temperature while still under the poling field and were aged for at least 24 h prior to piezoelectric and dielectric testing. To facilitate electrical characterization, silver (Ag) electrodes were applied to both sides of the films using a brush.

KNN Crystallographic Analysis: X-ray diffraction (XRD) was used to characterize and extract diffraction data for the crystal structure of KNN powders using a Bruker D8 Advance X-ray diffractometer (Bruker AXS Inc., Karlsruhe, Germany, using Co-K with EVA software). The peaks produced were analyzed using QUALX, a program for phase identification using powder diffraction data.

KNN Particle Size: Particle size was measured via laser scanning electron microscopy (SEM).

Microstructural Analysis: Ceramic particle spatial distribution and alignment were visualized and recorded at varying magnifications using SEM using a field-emission scanning electron microscope (SEM, Hitachi SU3900).

Topological Analysis: Surface properties of 10 vol% KNN-PDMS composites were characterized using atomic force microscopy (AFM) by tapping-mode AFM (TM-AFM, Agilent 5500).

Dielectric and Piezoelectric Properties: The dielectric response of the PDEP produced composite scaffolds was tested using a 1260 A Impedance/Gain-Phase Analyzer (Solartron Analytical, UK). The composites were examined in the frequency range from 0.1 Hz to 100 kHz at room temperature. The d_{33} piezoelectric coefficients of the composites were measured after each poling step at 97 Hz using a PiezoTest Berlincourt piezometer.

In Vitro Neural Stem Cell (NSC) Studies: The composition of the neurosphere (NSM), monolayer (MLM), and differentiation (DM) medias and blocking solution can be found in Table S1, Supporting Information.

Sample Preparation: Samples were plated in 24-well plates and washed in 70 vol% IPA and PBS (≈700 μL/well) three times, respectively, before cell culture.

NSC Culture: NSC culture: All animal experiments were approved by the Keele Animal Welfare and Ethical Review Body, where the approval number for the project is X350251A8. Neural stem cells (NSCs) were attained from days 1 to 3 postnatal mice. Mice were sacrificed via schedule 1 procedures in accordance with ASPA (1986). Mouse brains were dissected and kept in phosphate-buffered saline (PBS) and chilled in an ice box.

The subventricular zones of the all the brains was isolated using a scalpel and kept in 1 mL of NSM. The NSCs in the isolated zones were then dissociated with DNase I and cultured in T25 flasks in 5 mL of NSM. The flask was then incubated at 5% CO₂ and 37 °C, and NSCs were allowed to proliferate as neurospheres for 5 days. Neurospheres were dissociated into single cells with a DNase I/accutase mix (1:9) ready for plating onto samples.

NSC Studies: Samples and coverslips seeded with 700 µL of MLM at a density of 4.5×10^5 cells mL⁻¹. Once the cells on the coverslips were confluent, they were either fixed with 4% PFA for 1 h for assessment of NSC cytocompatibility studies or differentiated for 7 days by swapping the MLM to DM (with a 50% media change at day 3) for assessing effects of the samples on differentiation before fixation at day 5 and immunocytochemistry. Sample were purposefully left uncoated to unsure the effect of electrical stimulation was not masked by addition of surface proteins like laminin.

NSC Cytocompatibility Studies: Prior to fixing, some cells were stained for survival (live/dead) and proliferation (Edu) assays. Live/dead samples from each condition were incubated for 20 min with ethidium homodimer (6 µM), calcein-AM (4 µM), and DAPI (2 µL mL⁻¹) diluted in DMEM. After incubation, cells were washed once with PBS and fixed with 4% PFA prior to imaging. For the proliferation assay samples from each condition were also incubated with Edu (1 µM), a thymidine analogue which chelates into the DNA of diving cells, for 6 h prior to fixing.

Immunocytochemistry: Samples fixed with PFA were incubated in blocking solution for 1 h. Following incubation, the blocking solution was replaced with primary antibodies in blocking solution at 4 °C for 24 h before washing three times in PBS.

To assess culture stemness, NSCs were stained for Sox-2 (1:1000) transcription factor found in stems cell and Nestin (1:200), a filament protein found in NSCs. To assess NSC differentiation, cultures were stained for Tuj-1 (1:1000), a neuronal cytoskeletal component, an MBP (1:200) myelin constituent produced by oligodendrocytes, GFAP (1:500), an astrocyte cytoskeletal protein, and DAPI (1:500) as a nuclear stain. Samples were then washed with PBS and then incubated with blocking solution for an additional 1 h before being replaced with secondary antibodies (1:200) in blocking solution and incubated at room temperature for 4 h. Samples were washed three times, left to soak in PBS overnight, and mounted with Vectashield mounting medium with DAPI.

Imaging and Statistical Analysis: The statistical analysis was conducted using GraphPad Prism, with all values reported as the mean ± standard deviation. To determine if there were any significant differences between groups, a one-way ANOVA test with the Bonferoni's multiple comparison test was performed. This test assumed a normal distribution and did not involve matching. A *p*-value below 0.05 was considered statistically significant for indicating differences between experimental groups. Each experiment had a minimum of three biological repeats ($n \geq 3$), with each mouse litter counted as one biological repeat.

Supporting Information

Supporting Information is available from the Wiley Online Library or from the author.

Acknowledgements

This research is funded by the RCH studentship through University of Bath Alumni. The authors would also like to acknowledge the support provided by the Centre for Sustainable and Circular Technologies (CSCT) at the University of Bath.

Conflict of Interest

The authors declare no conflict of interest.

Data Availability Statement

The data that support the findings of this study are available from the corresponding author upon reasonable request.

Keywords

composites, piezoelectric, tissue engineering

Received: May 30, 2023

Revised: September 8, 2023

Published online:

- [1] S. Pluchino, A. Quattrini, E. Brambilla, A. Gritti, G. Salani, G. Dina, R. Galli, U. del Carro, S. Amadio, A. Bergami, R. Furian, G. Comi, A. L. Vescovi, G. Martino, *Nature* **2003**, 422, 688.
- [2] D. Drago, C. Cossetti, N. Iraci, E. Gaude, G. Musco, A. Bachi, S. Pluchino, *Biochimie* **2013**, 95, 2271.
- [3] A. Trounson, C. McDonald, *Cell Stem Cell* **2015**, 17, 11.
- [4] E. Curtis, J. R. Martin, B. Gabel, N. Sidhu, T. K. Rzesiewicz, R. Mandeville, S. van Gorp, M. Leerink, T. Tadokoro, S. Marsala, C. Jamieson, M. Marsala, J. D. Ciacci, *Cell Stem Cell* **2018**, 22, 941.
- [5] A. D. Levi, K. D. Anderson, D. O. Okonkwo, P. Park, T. N. Bryce, S. N. Kurpad, B. Aarabi, J. Hsieh, K. Gant, *J. Neurotrauma* **2019**, 36, 891.
- [6] T. Suzuki, M. U. España, M. A. Nunes, V. Zhurov, W. Dermauw, M. Osakabe, T. V. Van Leeuwen, M. Grbic, V. Grbic, *PLoS One* **2017**, 12, e0180658.
- [7] A. I. Teixeira, S. Ilkhanizadeh, J. A. Wigenius, J. K. Duckworth, O. Inganäs, O. Hermanson, *Biomaterials* **2009**, 30, 4567.
- [8] I. Goganau, B. Sandner, N. Weidner, K. Fouad, A. Blesch, *Exp. Neurol.* **2018**, 300, 247.
- [9] A. L. Manthey, W. Liu, Z. X. Jiang, M. H. Kong Lee, J. Ji, K. F. So, J. S. Ming Lai, V. W. Hong Lee, K. Chiu, *Cell Transplant.* **2017**, 26, 949.
- [10] A. N. Koppes, K. W. Keating, A. L. McGregor, R. A. Koppes, K. R. Kearns, A. M. Ziemba, C. A. McKay, J. M. Zuidema, C. J. Rivet, R. J. Gilbert, D. M. Thompson, *Acta Biomater.* **2016**, 39, 34.
- [11] A. Marino, G. G. Genchi, V. Mattoli, G. Ciofani, *Nano Today* **2017**, 14, 9.
- [12] A. L. Wani, A. Ara, J. A. Usmani, *Interdiscip. Toxicol.* **2015**, 8, 55.
- [13] B. Tandon, J. J. Blaker, S. H. Cartmell, *Acta Biomater.* **2018**, 73, 1.
- [14] A. H. Rajabi, M. Jaffe, T. L. Arinze, *Acta Biomater.* **2015**, 24, 12.
- [15] K. Kapat, Q. T. H. Shubhra, M. Zhou, S. Leeuwenburgh, *Adv. Funct. Mater.* **2020**, 30, 1909045.
- [16] K. K. Poon, M. C. Wurm, D. M. Evans, M. A. Einarsrud, R. Lutz, J. Glaum, *J. Biomed. Mater. Res. B Appl. Biomater.* **2020**, 108, 1295.
- [17] V. Jarkov, S. J. Allan, C. Bowen, H. Khanbareh, *Int. Mater. Rev.* **2021**, 67, 683.
- [18] N. D. Leipzig, M. S. Shoichet, *Biomaterials* **2009**, 30, 6867.
- [19] H. Khanbareh, S. van der Zwaag, W. A. Groen, *Smart Mater. Struct.* **2014**, 23, 105030.
- [20] D. A. van den Ende, B. F. Bory, W. A. Groen, S. van der Zwaag, *J. Appl. Phys.* **2010**, 107, 024107.
- [21] H. Nili, N. G. Green, *Phys. Rev. E: Stat. Nonlinear Soft Matter Phys.* **2014**, 89, 063302.
- [22] B. D. Tierney, S. DasGupta, S. Choi, A. L.-M. Qureshi, S. Jian-Kui, L. Zhen-Xing, X. Li, S. Jin, K. Song, S. A. Wilson, G. M. Maistros, R. W. Whatmore, *J. Phys. D: Appl. Phys.* **2005**, 38, 175.
- [23] K. W. Kwok, S. T. Lau, C. K. Wong, F. G. Shin, *J. Phys. D: Appl. Phys.* **2007**, 40, 6818.

- [24] H. Khanbareh, S. van der Zwaag, W. A. Groen, *J. Intell. Mater. Syst. Struct.* **2017**, *28*, 2467.
- [25] X. Chen, X. Han, Q. D. Shen, *Adv. Electron. Mater.* **2017**, *3*, 1600460.
- [26] A. Altomare, N. Corriero, C. Cuocci, A. Falcicchio, A. Moliterni, R. Rizzi, *J. Appl. Crystallogr.* **2015**, *48*, 598.
- [27] A. Vaitkus, A. Merkys, S. Grazulis, *J. Appl. Crystallogr.* **2021**, *54*, 661.
- [28] B. Orayech, A. Faik, G. A. López, O. Fabelo, J. M. Igartua, *J. Appl. Crystallogr.* **2015**, *48*, 318.
- [29] N. H. Shaik, R. G. Reifenberger, A. Raman, M. Spletzer, R. Reifenberger, J. Legleiter, M. A. S. R. Saadi, B. Uluutku, C. H. Parvini, S. D. Solares, *Surf. Topogr.* **2020**, *8*, 045004.
- [30] S. E. van Kempen, H. Khanbareh, P. Groen, J. M. Hol, Z. S. van der, *J. Phys.: Mater.* **2019**, *3*, 014004.
- [31] D. B. Deutz, N. T. Mascarenhas, J. B. J. Schelen, D. M. de Leeuw, S. van der Zwaag, P. Groen, *Adv. Funct. Mater.* **2017**, *27*, 1700728
- [32] A. Mogas Barcons, D. M. Chari, C. F. Adams, *Mater. Sci. Eng. C* **2021**, *123*, 111931.
- [33] L. A. Flanagan, L. M. Rebaza, S. Derzic, P. H. Schwartz, E. S. Monuki, *J. Neurosci. Res.* **2006**, *83*, 845.
- [34] J. L. Drury, D. J. Mooney, *Biomaterials* **2003**, *24*, 4337.
- [35] G. G. Genchi, L. Ceseracciu, A. Marino, M. Labardi, S. Marras, F. Pignatelli, L. Bruschini, V. Mattoli, G. Ciofani, *Adv. Healthcare Mater.* **2016**, *5*, 1808.
- [36] M. Hoop, X. Z. Chen, A. Ferrari, F. Mushtaq, G. Ghazaryan, T. Tervoort, D. Poulidakos, B. Nelson, S. Pané, *Sci. Rep.* **2017**, *7*, 1.
- [37] Y. S. Lee, G. Collins, T. Livingston Arinzeh, *Acta Biomater.* **2011**, *7*, 3877.
- [38] N. Royo-Gascon, M. Winingen, J. I. Scheinbeim, B. L. Firestein, W. Craelius, *Ann. Biomed. Eng.* **2013**, *41*, 112.
- [39] G. Ciofani, S. Danti, D. D'Alessandro, L. Ricotti, S. Moscato, G. Bertoni, A. Falqui, S. Berrettini, M. Petrini, V. Mattoli, A. Menciassi, *ACS Nano* **2010**, *4*, 6267.
- [40] N. K. James, D. B. Deutz, R. K. Bose, S. van der Zwaag, P. Groen, *J. Am. Ceram. Soc.* **2016**, *99*, 3957.